BILINGUAL PUBLISHING GROUP

Research in Ecology

https://journals.bilpubgroup.com/index.php/re

ARTICLE

Removal of Malachite Green from a Snakehead Fishpond in a Closed-Ecology System for Dragon Fruit Cultivation

Duong Mai Linh [1,2] **,** ***Nguyen Le Minh Tri*** [1] **,** ***Nguyen Thi Phuong Thao*** [1] **,** ***Nguyen Viet Thang*** [1] **,** ***Tran Trung Kien*** [1] **,** ***Tran Thi Hieu*** [1*]

[1] *Institute for Environment and Resources, National University of Ho Chi Minh City, Ho Chi Minh 740500, Vietnam*

[2] *Faculty of Technology-Engineering-Environment, An Giang University, National University of Ho Chi Minh City, Long Xuyên 900000, Vietnam*

ABSTRACT

In this study, g-C_3N_4 was decorated with Graphene Quantum Dots (GQDs) by using a thermal treatment method. Longer hydrothermal treatment time resulted in larger GQDs, with an average diameter of about 22 nm. This study investigated the effects of the size of GQDs on the photocatalytic performance of malachite green (MG), an organic compound used in aquaculture to prevent parasites, fungi, and bacteria. The incorporation of GQDs resulted in a decrease in the band gaps of the GQDs-loaded g-C_3N_4 samples and minimized the weight loss of materials during synthesis. The g-C_3N_4 sample loaded with smaller sizes of GQDs showed a lower MG removal efficiency at the beginning of the light irradiation than that loaded with larger sizes of GQDs, but their MG removal efficiency almost reached an equal efficiency later. The study introduced an innovative approach for examining the size-dependent effects of GQDs on the structural and photocatalytic characteristics of g-C_3N_4-based photocatalysts, utilizing both comprehensive experimental and statistical analyses. The findings demonstrated that GQD size influenced the structure and photocatalytic activity of photocatalysts. GQDs-loaded g-C_3N_4 photocatalysts showed their ability to remove MG in wastewater from snakehead fish (*Channa striata*) in a zero-emission system for dragon fruit cultivation. The study also highlighted the potential application for reducing antimicrobial contamination in wastewater from aquaculture.

Keywords: Effect of Size; Quantum Dot; Malachite Green; Snakehead Fish Wastewater; Antimicrobial Contamination; Zero-Emission System

*CORRESPONDING AUTHOR:
Tran Thi Hieu, Institute for Environment and Resources, National University of Ho Chi Minh City, Ho Chi Minh 740500, Vietnam;
Email: hieutran.envi@gmail.com

ARTICLE INFO
Received: 4 February 2026 | Revised: 16 March 2026 | Accepted: 20 March 2026 | Published Online: 22 June 2026
DOI: https://doi.org/10.30564/re.v8i3.13127

CITATION
Linh, D.M., Tri, N.L.M., Thao, N.T.P., et al., 2026. Removal of Malachite Green from a Snakehead Fishpond in a Closed-Ecology System for Dragon Fruit Cultivation. Research in Ecology. 8(3): 313–327. DOI: https://doi.org/10.30564/re.v8i3.13127

1. Introduction

Climate change has been intensifying recently, causing detrimental effects on our environment. Some parts of the world have experienced unexpected floods driven by heavy rains, which destroyed crops, infrastructure, and human and animal lives. Meanwhile, other areas are facing severe droughts due to prolonged dry seasons, which are unfavorable for cultivating crops, raising animals, and protecting human health. Although three-fourths of the Earth's surface is covered by water, less than 3% of it is fresh and drinkable. Climate change has exacerbated the insecurity and insufficiency of our freshwater supplies. In addition, water pollution has posed a significant threat to water systems, such as lakes, rivers, and seas. In recent years, the growth of many industries and human activities has had a greater impact on the global economy, but it has also led to several harmful side effects on the environment. Pollutants such as dyes, pharmaceuticals, heavy metals, and persistent organic pollutants have been found in wastewater discharged from industrial and human activities. The demand for clean water has become more urgent due to the growing global population and industrialization. Dyes released from industries such as plastic, leather, textiles, printing, paper, and food are colored compounds containing chromophores and auxochromes. More than 30,000 t of dyes have been released into water systems, causing detrimental effects on aquatic life due to their high toxicity, stemming from their carcinogenic and mutagenic nature.

Malachite green (MG), an organic dye known by its IUPAC designation N-methyl-di-amino-tri-phenyl-methane, has been employed in the coloration of textiles, including jute, silk, cotton, wool, and leather [1]. Additionally, it was found that MG was used in aquaculture to prevent parasites, fungi, and bacteria [2–4]. In 2012, Khodabakhshi and Amin, using liquid chromatography-mass spectrometry (LC-MS), determined the concentration of MG in the effluents of a fish farm to be in the range of 0.0057 to 384 $\mu g \cdot L^{-1}$ [5]. The report by Kwan et al. also revealed the presence of MG in fish tissue [6]. More recently, Kwan et al. employed potentiometry with ion-selective electrodes (ISE) to detect MG in aquaculture wastewater from a fish farm. They reported that the concentration of MG ranged from 4.90×10^{-4} to 4.97×10^{-5} $mol \cdot L^{-1}$ [7]. Although MG has been used in aquaculture due to its low cost and high availability, it has never been approved as a veterinary medicine for food-producing animals because it causes detrimental effects on humans, such as eye irritation, headaches, and illnesses affecting the heart, liver, and brain [2,8]. Thus, the presence of MG in effluents discharged from aquaculture systems is a cause for concern [9]. Therefore, there is an urgent need to treat wastewater containing dyes using modern technologies. These techno-management practices are particularly crucial for the integrated farming zero-emission systems where wastewater from aquacultural ponds is used for agricultural production [10,11].

Several methods have been employed to treat dyes and pharmaceuticals in aqueous effluents, such as adsorption, electrochemistry, ozonization, flocculation, coagulation, biological methods, ion exchange, sonochemical degradation, and photocatalysis [12,13]. Among these, active-radical-based photocatalysis is regarded as an effective method for the degradation of organic pollutants, as it minimizes serious secondary pollution emissions. This approach is quite effective, requiring simple procedures and low operational costs. Photocatalysts are key components of photolysis. Numerous photocatalysts have been used for environmental applications, such as $Bi_2WZnTiO_9$, $CuInS_2$, p-$CuAl_2O_4$/n-YVO_4 heterojunction, Ag_2WO_4/ZIF-8, etc. [14–17]. Over the past decade, graphitic carbon nitride (g-C_3N_4), a non-metallic semiconductor, has demonstrated its potential for environmental applications [18,19]. It can be fabricated from low-cost carbon and nitrogen sources and possesses various properties, such as thermal stability (up to 600 °C), super-hardness, and high resistance to water and chemicals [20,21]. As a photocatalyst, g-C_3N_4 extends its light absorption into the visible light range due to its band-gap energy (~2.8 eV). However, its low surface area, low porosity, and limited absorption of solar light hinder its photocatalytic performance. To improve the photocatalytic activity of g-C_3N_4, the decoration of g-C_3N_4 with other materials has been explored [22–25]. Graphene quantum dots (GQDs) are carbon-based nanomaterials less than 100 nm in size [26,27]. They exhibit low toxicity, good photoluminescence, chemical stability, and an effective quantum confinement effect [28,29]. As a result, GQDs have been applied in biological, energy, optoelectronic, and environmental fields [30]. As carbon derivatives, GQDs accumulate elec-

trons on their surfaces [28]. They are also chemically and physically stable and have a high surface-to-mass ratio due to functional groups at their edges [31,32]. It is noteworthy that scientists can tune the optical properties of GQDs by altering their morphologies. For these reasons, decorating g-C_3N_4 with GQDs can improve its optical properties.

Although scientists have paid attention to the decoration of g-C_3N_4 with quantum-dot materials, there are concerns related to the effects of GQD size on the photocatalytic performance of g-C_3N_4 in the photodegradation of MG. Therefore, in this study, we conducted the decoration of g-C_3N_4 with GQDs and investigated the effects of their sizes on structural properties and photocatalytic activity of g-C_3N_4 in the degradation of MG under UV light irradiation. We also studied the impact of the pH of the solution, the factor that determined the surface charge properties of materials, on its degradation. Furthermore, this study evaluated the effectiveness of a GQDs-loaded g-C_3N_4 photocatalyst for the removal of MG from simulated effluent sourced from a snakehead fishpond within a zero-emission system used in dragon fruit cultivation, under UV light irradiation. To our knowledge, there are a few studies focusing on mild fabrication methods for GQDs-loaded g-C_3N_4 photocatalysts that preserve the porosity of g-C_3N_4 templates to boost MG photodegradation in wastewater originating from snakehead fishponds. Additionally, this work introduces an innovative approach for examining the size-dependent effects of GQDs on the structural and photocatalytic properties of g-C_3N_4-based photocatalysts, utilizing both comprehensive experimental and statistical analyses.

2. Experimental Section

2.1. Synthesis of GQDs

We synthesized GQDs via a hydrothermal treatment of 1 g of glucose dissolved in 100 mL of distilled (DI) water. The solution was stored in a Teflon-lined autoclave. The GQDs solution was obtained by subjecting the mixture to heat treatment at 160 ℃ for varying durations (4 h, 6 h, and 8 h), followed by purification using a dialysis tube (molecular weight cut-off (MWCO) ~ 10,000 Da, Millipore). The obtained GQDs were denoted as GQD-4, GQD-6 and GQD-8.

2.2. Synthesis of g-C_3N_4 and Its Decoration with GQDs

We synthesized g-C_3N_4 through the heat treatment of dicyanamide in a furnace at 550 ℃ ± 1 ℃ with a heating rate of 1 ℃/min. For the decoration of g-C_3N_4 with GQDs, dicyanamide was separately mixed with different 5 mL GQDs solutions. The mixtures were placed in a covered crucible and calcined at 1 ℃/min to yield GQD-loaded g-C_3N_4 samples, labeled as GQD-4@g-C_3N_4, GQD-6@g-C_3N_4, and GQD-8@g-C_3N_4. **Figure 1** illustrates the synthesis of GQDs-loaded g-C_3N_4 samples.

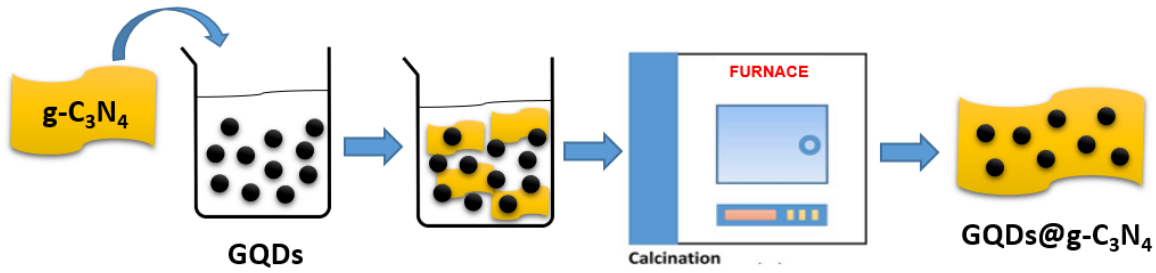

Figure 1. The decoration of g-C_3N_4 with GQDs.

2.3. Characterization of Photocatalysts

We employed a Transmission electron microscope (TEM) to study the morphologies of the photocatalysts. Additionally, we analyzed their crystal structures using X-ray diffraction (XRD), performed with an X-ray diffractometer equipped with Cu Kα radiation (λ = 0.154056 nm). The optical properties of the samples were elucidated through Diffuse reflectance spectra (DRS) recorded in the wavelength range of 200–800 nm. Photoluminescence (PL)

spectra were measured on a luminescence spectrometer (F-7000, Hitachi) with a solid accessory at room temperature and an excitation wavelength of 375 nm. The thermal stability of the samples was studied on a thermogravimetric analysis (TGA) instrument. The specific Brunauer–Emmett–Teller (BET) surface area and pore size measurements of samples were conducted on a Quantachrome apparatus at 77.3 K under nitrogen gas. Before the BET measurement, the samples were degassed in a flow of N2 at 300 ℃ for 5 h. The specific surface area was determined by the Brunauer–Emmett–Teller method. The pore size distribution was calculated using Barrett–Joyner–Halenda (BJH) desorption branches of the isotherms.

2.4. The Study of the Photocatalytic Reaction of MG

To study the photocatalytic activity of the synthesized materials, 80 mg of photocatalysts were added to a beaker containing 50 mL of a solution of MG with a certain concentration to make a suspended solution. After stirring the solution in the dark for 90 min to achieve the adsorption-desorption equilibrium, we turned on the UV-LED (lightemitting diode) lamp (365 nm, 95 mW/cm^2, 1.75 × 10^{21} photons/cm^2·s) to illuminate the solution for 120 min under stirring to observe the degradation of MG. To adjust the pH of the solution, 0.1 M NaOH or HCl was added to the solution of MG. After 30 min of the photocatalytic reaction, we took 3.0 mL of the MG solution out of the beaker for centrifugation at a rate of 3,000 rpm for 3 min before determining the MG remaining concentration, using a UV-Vis spectrometer [33]. The photocatalytic degradation efficiency (R, %) of MG was calculated using Equation (1):

$$R\,(\%) = (C_0 - C_t) \times 100/C_0 \quad (1)$$

Where, C_0 represents the initial concentration of MG (mg/L), while C_t denotes the concentration of MG at time t (min). All experiments were conducted in triplicate.

2.5. Application of Photocatalytic Degradation of MG in the Wastewater from Snakehead Fishpond

To study the photodegradation of MG in fish-farming wastewater over the photocatalysts, 11.4 mg·L^{-1} MG was added to 50 mL of the wastewater taken from a snakehead fishpond of a local farm (**Figure 2**). Before the addition of MG, the wastewater was left 24 h for sedimentation. The wastewater containing MG was then exposed to UV light in the presence of 80 mg of photocatalysts for 120 min. Determination of the remaining MG concentration followed the same procedure as Section 2.4.

Figure 2. Snakehead fish wastewater is utilized within a zero-emission system for the cultivation of dragon fruit.

3. Results and Discussion

3.1. Study of Material Characterization

Figure 3 showed the morphologies and size distribution of GQDs after the hydrothermal treatment at different intervals of time. It can be observed that a longer time of hydrothermal treatment resulted in a larger size of GQDs with an average diameter of about 22 nm. There was no significant difference in particle size or size distribution between GQDs obtained after 6 h and those obtained after 8 h. In contrast, GQDs synthesized in 4 h exhibited much smaller sizes and a narrower size distribution. The similarity in particle size and size distribution between GQDs obtained after 6 h and 8 h suggests that glucose molecules primarily assembled into GQDs. The hydrothermal method for synthesizing GQDs is a bottom-up approach, where GQDs are formed by the assembly of smaller glucose molecules. When a certain amount of glucose is added to the solution, it takes time for the smaller glucose molecules to self-assemble into GQDs.

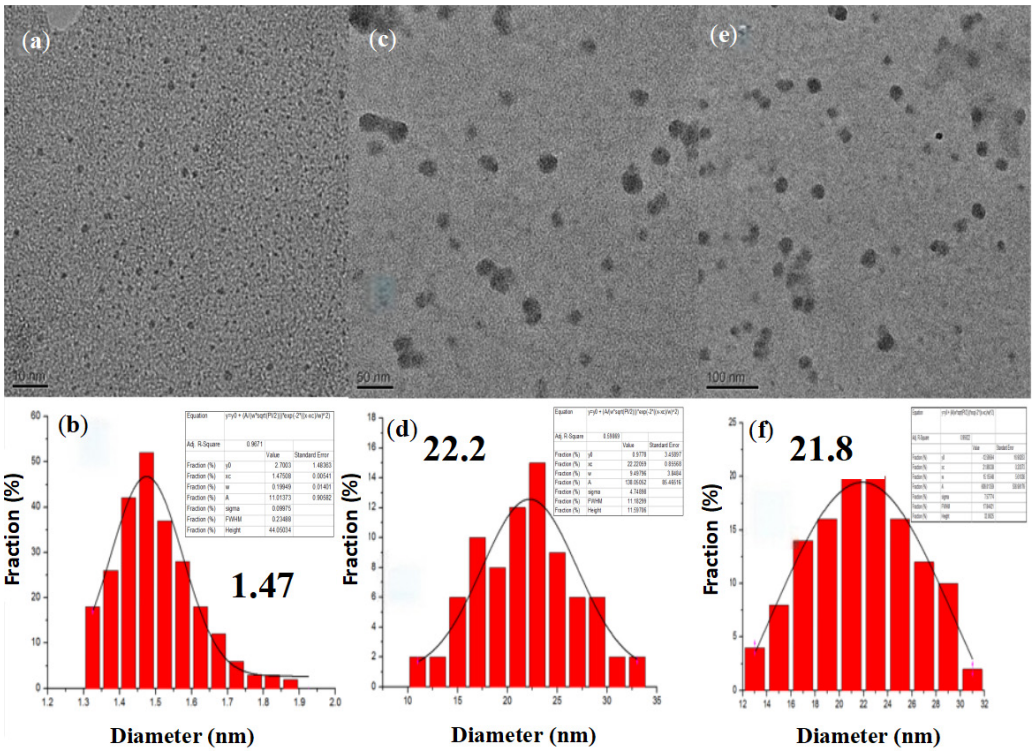

Figure 3. The structures and size distributions of the GQDs were characterized at various hydrothermal treatment durations: (**a**,**b**) 4 h, (**c**,**d**) 6 h, and (**e**,**f**) 8 h [33].

The hydrothermal treatment time affected the visible-light harvesting ability of GQDs as we can see an increase in the visible-light absorbance of GQDs and their red-shifts of absorption wavelength after a long hydrothermal treatment time (**Figure 4a**). The absorption region below 300 nm is related to the π–π^* transition in aromatic C=C carbons of GQDs, while the region above 300 nm corresponds to the n–π^* transition in the C=O carbon core and C=O surface state transition of GQDs [34]. Both GQD-6 and GQD-8 showed equivalent absorbance, which is higher than that of GQDs-4 in visible light, due to their equivalent particle sizes.

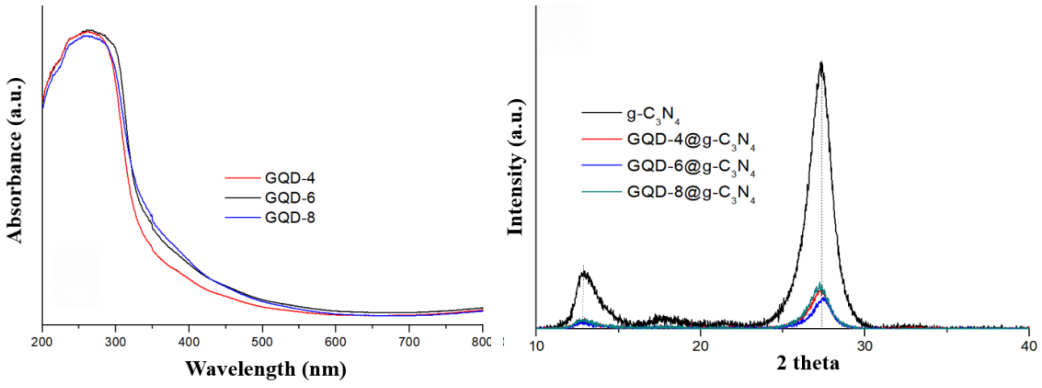

Figure 4. (**a**) The UV-VIS spectra of GQDs and (**b**) XRD patterns of g-C_3N_4 and GQDs-loaded g-C_3N_4 samples.

After the decoration of g-C_3N_4 with GQDs, the XRD patterns of all GQDs-loaded g-C_3N_4 samples showed all characteristic peaks of g-C_3N_4, which are located at around 2θ = 27.4° and 12.8° (Joint Committee on Powder Diffraction Standards (JCPDS) No. 87–1526) (**Figure 4b** and **Figure S1**) [35,36]. The former peak is indicative of

stacking interlayered heptazine (C_6H_7) units, while the latter is indicative of in-planar nitrogen pores in the structure of g-C_3N_4 [37,38]. When we investigated GQDs-loaded g-C_3N_4 samples, their weaker intensities and lower angles of those peaks showed that the successful incorporation of GQDs into the g-C_3N_4 lattice broadened the distance between g-C_3N_4 layers and also between nitrogen pores [33]. The incorporation of GQDs resulted in the band gaps of the GQDs-loaded g-C_3N_4 samples becoming narrower after the modification. According to the Kubelka–Munck theory, the bandgap values of those samples were determined as 2.81 eV, 2.79 eV, 2.77 eV, 2.74 eV for g-C_3N_4, GQD-4@g-C_3N_4, GQD-6@g-C_3N_4 and GQD-8@g-C_3N_4, respectively [33]. The light absorption ability of GQDs-loaded g-C_3N_4 samples in both the UV and visible regions increased after the incorporation of GQDs (**Figure 5a**). Moreover, TGA analysis indicated that the deposition of GQDs reduced the weight loss of the dicyanamide precursor during the synthesis of GQDs-loaded g-C_3N_4 samples, thus increasing their thermal stability compared to g-C_3N_4 (**Figure S2**). Scanning electron microscope (SEM) images in **Figure S3** showed that the morphologies of GQD-6@g-C_3N_4 and g-C_3N_4 exhibited the presence of clusters of particles. The loading of GQDs on g-C_3N_4 resulted in an increase in the surface area and pore volume of the bulk g-C_3N_4 (**Table 1**) due to the exfoliation of the bulk g-C_3N_4, which is consistent with the report of Jiao et al. [39]. However, this study showed that the incorporation of GQDs would retain the meso-porous structure of the bulk g-C_3N_4 and its pore diameter (**Table 1**). The bulk g-C_3N_4 exhibited a meso-porous structure with cylindrical pores, which were characterized by the type-IV isotherms of g-C_3N_4 with H3 hysteresis loops in the P/P_0 range of 0.4–1.0. In addition to mesopores, macropores were also present in bulk g-C_3N_4, which is proved by the adsorption edges of those isotherms within the P/P_0 region of 0.8–1.0 (**Figure S4**).

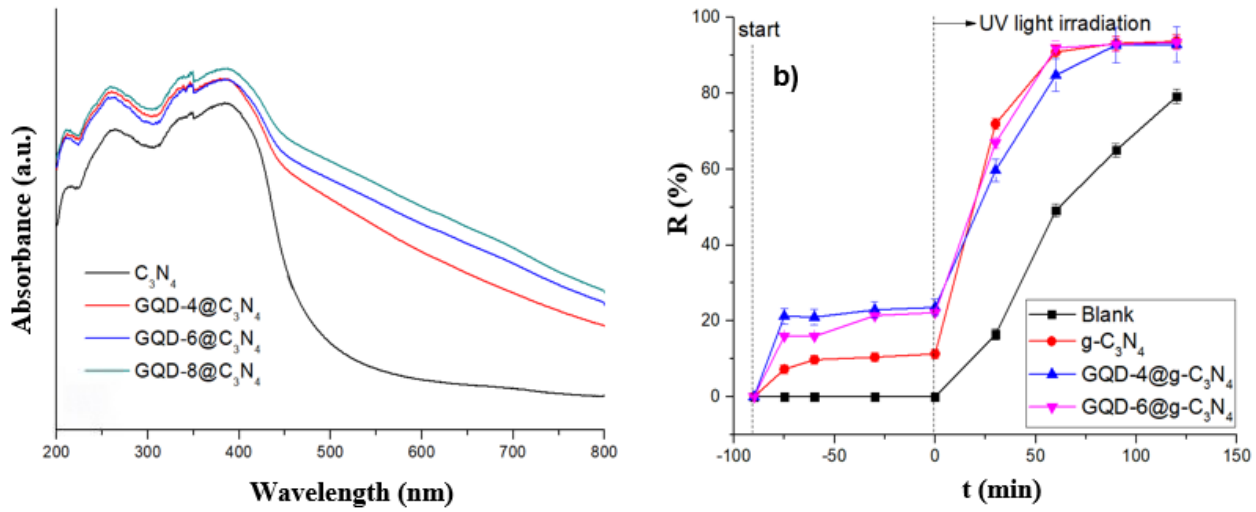

Figure 5. (**a**) UV-VIS spectra of GQDs-loaded g-C_3N_4 samples; (**b**) Degradation of MG by g-C_3N_4 and GQDs-loaded g-C_3N_4 samples.

Table 1. BET parameters of the photocatalysts [33].

Sample	Surface Area ($m^2 \cdot g^{-1}$)	Pore Volume ($cm^3 \cdot g^{-1}$)	Pore Diameter (nm)
g-C_3N_4	14.22	0.066	4.0
GQD-4@g-C_3N_4	28.51	0.109	4.0
GQD-6@g-C_3N_4	27.61	0.123	4.0

3.2. Abatement of MG over the Photocatalysts

3.2.1. Effects of Size of GQDs

The abatement of MG over the photocatalysts was conducted under UV light irradiation. g-C_3N_4, GQD-4@g-C_3N_4, and GQD-6@g-C_3N_4 were used as representative photocatalysts for the photocatalytic abatement of MG. As shown in **Figure 5b**, 80% of MG was degraded by photolysis after 120 min of irradiation without the addition of the photocatalysts, indicating that the photolysis of MG occurred under UV light irradiation. In the presence of g-C_3N_4, 93% of MG was removed through adsorption, photocatalysis, and photolysis after 120 min of UV light irradiation. After decorating g-C_3N_4 with GQDs, both GQD-4@g-C_3N_4 and GQD-6@g-C_3N_4 showed enhanced adsorption of MG, with 20% of MG being abated in the dark. This can be attributed to the higher surface area of the GQD-loaded g-C_3N_4 samples and the presence of carbonyl groups contributed by the GQDs [40,41]. These functional groups create negative charges that attract the positively charged parts of MG molecules through electrostatic interaction on the surface of the GQD-loaded g-C_3N_4 samples [41,42]. Meanwhile, the photocatalytic degradation of MG over g-C_3N_4, GQD-4@g-C_3N_4, and GQD-6@g-C_3N_4 exhibited high efficiency, with more than 90% of MG being removed. For the GQD-loaded g-C_3N_4 samples, GQD-4@g-C_3N_4 showed lower MG removal efficiency in the first 50 min of light irradiation compared to GQD-6@g-C_3N_4, but its MG removal efficiency later matched that of GQD-6@g-C_3N_4. The photocatalytic and adsorption properties of GQD-6@g-C_3N_4, as a representative of GQD-loaded g-C_3N_4 samples, were further investigated by examining the effects of the solution pH, which influences the surface charges of materials [42].

3.2.2. Effects of pH

The pH of the solution governs the chemical species of MG present. **Figure 6a** presents the UV-VIS spectra of MG across various pH levels, evaluated both in darkness and under UV irradiation, in the absence of photocatalysts. It is reported that the pKa value of MG is 6.9. When pH < pKa, MG molecules exist as anions, but they become cations when pH > pKa [43]. The pH-dependent chemical species of MG influenced its UV-VIS absorption. As seen in **Figure 6a**, the intensity of the main peak at 618 nm changes with pH, but there is no shift in the peak position, indicating a change in the electron density of the chromophore ring structure of MG due to alterations in the bond orbital energy of the MG molecules. Moreover, the intensity of the main peak decreases with an increase in pH under UV light irradiation. This phenomenon becomes more pronounced as the pH increases from 2 to 10, suggesting that the degradation of the chromophore ring structure of MG occurs even without the presence of photocatalysts. More than 80% of MG in the solution underwent photolysis across the entire pH range after 120 min of UV light irradiation (**Figure 6b**). In the presence of g-C_3N_4 and under dark conditions, the UV-VIS spectra of the MG solution (pH = 4, no pH adjustment) showed a decrease in the intensity of the main peak, due to the accumulation of MG on g-C_3N_4 (**Figure 6e**). The decrease was more pronounced at pH above 6, as positively charged MG molecules were attracted to the negatively charged g-C_3N_4 surface, whose point of zero charge (PZC) was 2.5 [44]. In contrast, the adsorption efficiency of MG decreased in acidic media due to the competitive adsorption of H^+ ions with MG molecules (**Figure 6f**). A similar interpretation applies to the pH-dependent adsorption of GQD-6@g-C_3N_4. GQD-6@g-C_3N_4 exhibited enhanced adsorption compared to g-C_3N_4. The presence of GQD-6@g-C_3N_4 also boosted the degradation of MG, with more than 90% of MG degraded within 60 min across the entire pH range (**Figure 6c,d**). The photocatalytic performance of GQD-6@g-C_3N_4 in the degradation of MG is comparable to that of other g-C_3N_4-based photocatalysts (**Table 2**). The results indicate that photolysis of MG is more favorable in alkaline media. Additionally, the decoration of g-C_3N_4 with GQDs enhances MG abatement from the solution. Interestingly, there are blue shifts in the main peak of the UV-VIS spectra of both g-C_3N_4 and GQD-6@g-C_3N_4 (**Figure 6c,e**), which suggest the de-methylation of MG molecules during their photocatalytic degradation [45].

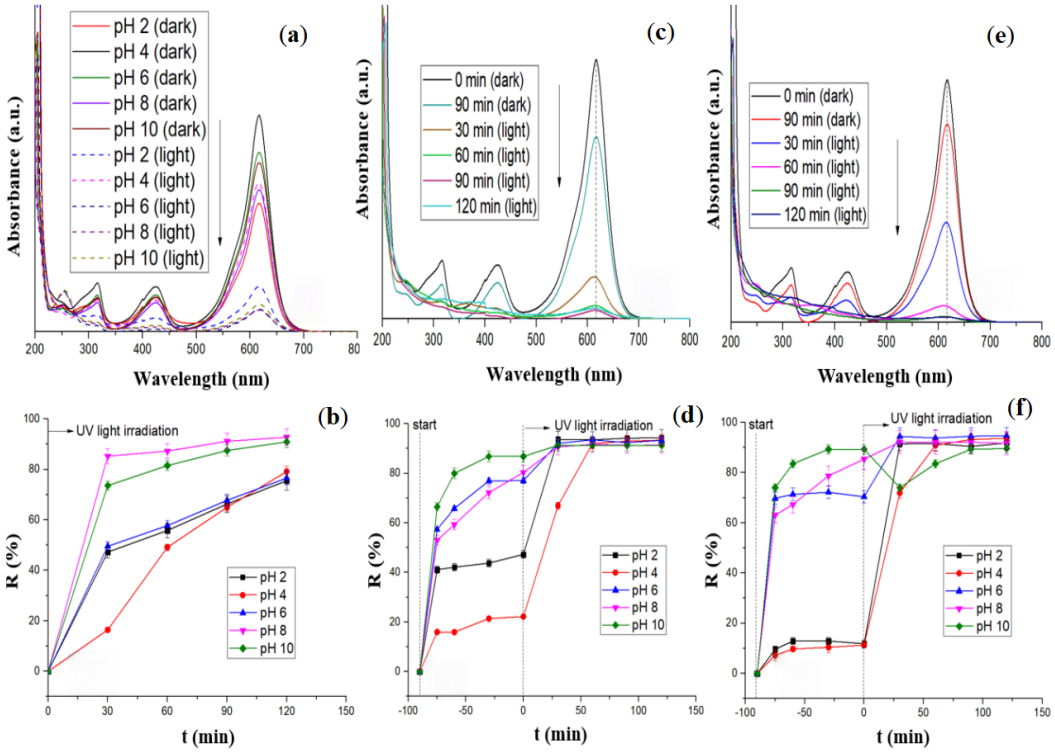

Figure 6. (**a**,**b**) The abatement of MG without photocatalysts, and (**c**,**d**) in the presence of GQD-6@g-C_3N_4, and (e,f) g-C_3N_4.

Table 2. Photo-degradation efficiency of MG over g-C_3N_4-based photocatalysts.

No.	Photocatalyst	Experimental Conditions	Max. Efficiency (%)/Time (min)/Rate Constant (min^{-1})	Ref.
1.	C-CeO_2/g-C_3N_4 nanocomposite	Batch mode; sunlight; catalyst dosage: 0.5 $g·L^{-1}$; MG concentration: 10 $mg·L^{-1}$	92/150/12 × 10^{-3} – 15 × 10^{-3}	Madona et al. [46]
2.	Carbon-coated tungsten-doped molybdenum oxide nanowires	Batch mode; Xe arc lamp; catalyst dosage: 0.5 $g·L^{-1}$; MG concentration: 5 $mg·L^{-1}$	92/120/9 × 10^{-3}	Shaheen et al. [47]
3.	PSCN/Ag@AgI/WO_3	Batch mode; Xe arc lamp; catalyst dosage: 0.5 $g·L^{-1}$; MG concentration: 10 $mg·L^{-1}$	90/60/12 × 10^{-3} – 15 × 10^{-3}	Hasija et al. [48]
4.	$BiFeO_3$/g-C_3N_4	Batch mode; sunlight; catalyst dosage: 0.5 $g·L^{-1}$; MG concentration: 10 $mg·L^{-1}$	86/50/12 × 10^{-3} – 15 × 10^{-3}	Mohanty et al. [49]
5.	TiO_2 NP	Batch mode; UV; catalyst dosage: 1.0 $g·L^{-1}$; MG concentration: 20 $mg·L^{-1}$	100/180/10^{-3} – 10^{-2}	Salehzadeh et al. [50]
6.	GQD@g-C_3N_4	Batch mode; LED; catalyst dosage: 1.6 $g·L^{-1}$; MG concentration: 20 $mg·L^{-1}$	93/120/29× 10^{-3} – 31 × 10^{-3}	This study

3.2.3. Kinetics of the Photodegradation of MG over the Photocatalysts

Rate constants of the photodegradation of MG over different photocatalysts are shown in **Figure 7a**. Those parameters were calculated by using the following pseudo-first-order kinetic models as described by Equation (2) [33]:

$$ln\frac{C_0}{C} = kt \quad (2)$$

Where, t represents the irradiation time (min); C_0 and C ($mg·L^{-1}$) represent the initial and final concentration of MG, respectively; k (min^{-1}) represents the reaction rate constant.

The photodegradation of MG over g-C_3N_4, GQD-4@g-C_3N_4, and GQD-6@g-C_3N_4 photocatalysts had greater rate constants than their photolysis at pH = 4, indicating that the photocatalysts boosted the degradation of MG at the studied pH. Moreover, the rate constants of the photo-

catalysis driven by GQDs loaded g-C_3N_4 samples are approximately that of the photocatalysis driven by g-C_3N_4.

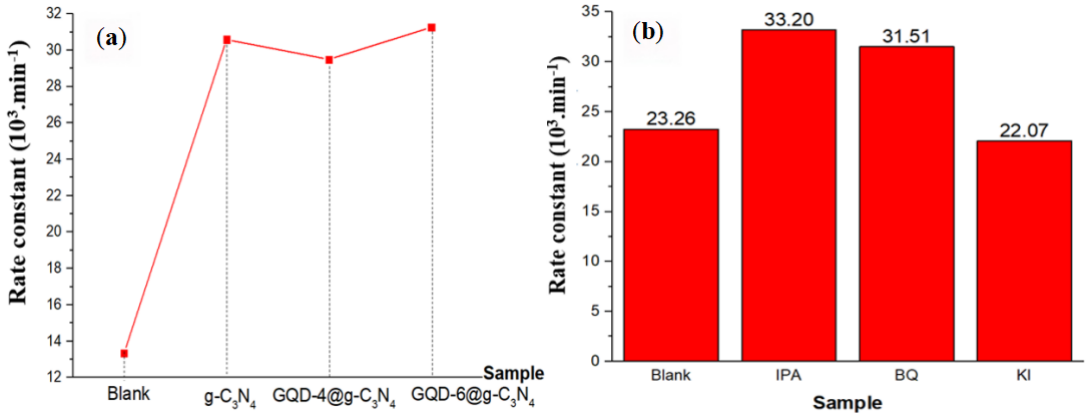

Figure 7. (**a**) The rate of MG photodegradation over different photocatalysts. (**b**) Rate constants for the photodegradation of MG by GQD-6@g-C_3N_4 in the presence of various quenching agents.

3.2.4. Photocatalytic Mechanism of MG over Photocatalysts

In this section, we discussed the photocatalytic mechanism of MG driven by radical species. We performed the photocatalytic degradation of MG under UV light irradiation in the presence of GQD-6@g-C_3N_4 with the addition of 1 mL of different quenchers, such as Isopropyl Alcohol (IPA), Ethylenediaminetetraacetate (EDTA) and Benzoquinone (BQ), which acted as the quenchers of •OH, h^+ and $•O_2^-$, respectively [51]. As seen in **Figure 7b**, the abatement of MG over GQD-6@g-C_3N_4 became slower with a lower rate constant as Benzoquinone (BQ) was added to the solution. It implies that $•O_2^-$ was the dominant radical that suppressed the photocatalytic degradation of MG.

To further study the photocatalytic mechanism of MG over the photocatalysts, we calculated the potentials of the conduction band (CB) and valence band (VB) of g-C_3N_4 by using the following Equations (3) and (4):

$$E_{VB} = \chi - E_e + 0.5E_g \quad (3)$$

$$E_{CB} = E_{VB} - E_g \quad (4)$$

Where, χ denotes the semiconductor's electronegativity (4.72 e), E_e is the free electron energy (4.5 eV vs. normal hydrogen electrode (NHE)), and E_g is the band gap energy at 2.81 eV [33]. Therefore, the conduction band edge (E_{CB}) and valence band edge (E_{VB}) of g-C_3N_4 were determined to be −1.19 eV and 1.62 eV, respectively. Upon light irradiation, photoexcited electrons (e^-) were generated in the conduction band (CB), while holes (h^+) were produced in the valence band (VB) of g-C_3N_4. The electrons subsequently reacted with dissolved O_2 molecules in the solution to produce $•O_2^-$ radicals, whereas the holes participated in the oxidation of MG, as illustrated in **Figure S5**. The deposition of GQDs, which functioned as a photosensitizer, on the g-C_3N_4 would enhance the photocatalytic activity of g-C_3N_4. The radical-driven photocatalytic degradation of MG was shown in Equations (5)–(9):

$$g\text{-}C_3N_4 + h\nu \rightarrow e^- (CB) + h^+ (VB) \quad (5)$$

$$GQDs + h\nu \rightarrow e^- (CB) + h^+ (VB) \quad (6)$$

$$O_2 + e^- \rightarrow •O_2^- \quad (7)$$

$$•O_2^- + H_2O \rightarrow •OH + OH^- \quad (8)$$

$$•O_2^-/•OH/\ h^+ + MG \rightarrow \text{degradation products} \quad (9)$$

PL measurement is a way to study the separation of electrons and holes in photocatalysts. A high recombination rate of electrons and holes would lead to a high intensity of the strongest emission peaks in PL spectra [52]. As shown in **Figure S6**, the GQDs-loaded g-C_3N_4 samples showed better suppression of photo-induced charge carriers than the g-C_3N_4, which contributed to the enhanced photocatalytic performance of the GQDs-loaded g-C_3N_4 [53]. Moreover, the redshifts of the strongest emission peaks in the PL spectra of the GQDs loaded g-C_3N_4 samples from 454 nm to 472 nm may be ascribed to the formation of N-doped graphitic carbon in the g-C_3N_4 framework, causing the π-electron delocalization in the conjugated g-C_3N_4 framework [54].

The incorporation of graphitic nitrogen made the color of g-C_3N_4 change from yellow to brown (**Figure S7**). The results indicated that the deposition of GQDs facilitated the doping of nitrogen heteroatoms into the g-C_3N_4 structure, driven by the release of NH_3 during the polycondensation of the dicyanamide precursor (**Figure S2**).

3.3. Size-Dependent Effects of GQDs on the Structure and Photocatalytic Activity of Photocatalysts

To investigate the size-dependent effects of GQDs on the structural and photocatalytic properties of photocatalysts, Pearson correlation analyses were conducted between GQD size and various parameters, including surface area, pore volume, pore diameter, band-gap energy, MG removal efficiency, and the rate constant for MG photocatalytic degradation using SPSS 22.0 software. As summarized in **Table 3**, all examined parameters exhibited non-zero Pearson correlation coefficients, suggesting a dependence of both structure and photocatalytic activity on GQD size. The analysis indicated a non-linear relationship between these characteristics and GQD size. Surface area, pore volume, band-gap energy, and the rate constant for MG degradation demonstrated strong correlations with GQD size, whereas pore diameter and MG removal efficiency were moderately and weakly correlated, respectively. With the exception of pore diameter and band-gap energy, all parameters showed positive correlations with GQD size. These findings demonstrate that GQD size influenced the structure and photocatalytic activity of photocatalysts.

Table 3. Pearson correlation (*r*) of studied parameters with the size of GQDs.

Parameter	Surface Area	Pore Volume	Pore Diameter	Band-Gap Energy	Removal Efficiency	Rate Constant
Size of GQDs	0.50[a]	0.73[a]	−0.35[b]	−0.89[a]	0.093[c]	0.50[a]

Note: Correlation is significant at the 0.01 level. [a] Strong correlation ($|r| \geq 0.5$); [b] Moderate correlation ($0.3 < 0.5$); [c] Weak correlation ($|r| \leq 0.3$).

3.4. Applications for Snakehead Fish Wastewater in a Zero-Emission System for Dragon Fruit Cultivation

The wastewater from the snakehead fishpond was collected from a zero-emission system for dragon fruit farming with a total pond area of 3,100 m^2, a depth of 1.7 m, and a total pond volume of 5,270 m^3. The snakehead fish cultivation density is 100 fish per square meter, with a cultivation period of 4 to 5 months. The survival rate stands at 80%, and each fish weighs approximately 600 g. The average yield is 50 kg per square meter. Water changes account for 20% of the total pond volume, at one time in the first month and two times each month from the second to the fifth month. Before the addition of MG, the wastewater was left for 24 h for sedimentation. 50 mL of wastewater was decanted, followed by the addition of MG. **Figure 8a** shows the abatement of MG under ultraviolet (UV) light irradiation after the addition of 80 mg of GQD-6@g-C_3N_4 to the simulated wastewater. Accordingly, 91% of MG was abated from wastewater after 120 min of light irradiation. The UV-VIS spectra exhibited an intensive decrease in the peak intensity of the main peak of MG at about 618 nm, and its blue shift after 120 min of the light irradiation, which is indicative of the process of *N*-demethylation during the photodegradation of MG [55]. Moreover, a decline in the absorbance of the peaks at 425 and 315 nm of the UV-VIS spectra is evidence of the destruction of the chromophore structure of MG. Additionally, a new absorbance peak appears at about 360 nm in the spectra of MG, which illustrates the formation of DLBP as one of the main products of the decomposition of MG [55] (**Figure 8b**). The disappearance of this compound in the UV range after 120 min of UV light irradiation is the indicator of the complete decomposition of DLBP. Benzophenone compounds are potentially to cause carcinogenesis, sensitization, and endocrine disruption [56,57]. Therefore, the complete decomposition of DLBP would reduce the toxicity of MG solutions. Previous studies showed that the photocatalytic decomposition of MG was favorable at low concentration [58]. However, according to **Figure 8c**, the rate constant of the photodegradation of MG in the wastewater matrix at lower concentrations of MG was lower than that of MG at its higher concentration, indicating unfavorable decomposition of MG in the wastewater matrix. Nitrogen, phosphorus and organic matters in aquaculture wastewater would consume reactive species during the photodegradation of

MG [59]. Moreover, according to **Figure 8c**, there was no spectral interference in the matrix of the pristine wastewater. Thus, although the wastewater matrix hindered the light-driven oxidation of MG, it caused no spectral interference in the UV-VIS measurement. The results revealed the ability of GQDs-loaded g-C_3N_4 photocatalysts to abate MG in the simulated wastewater and the potential interference of the sample matrix in the abatement of MG.

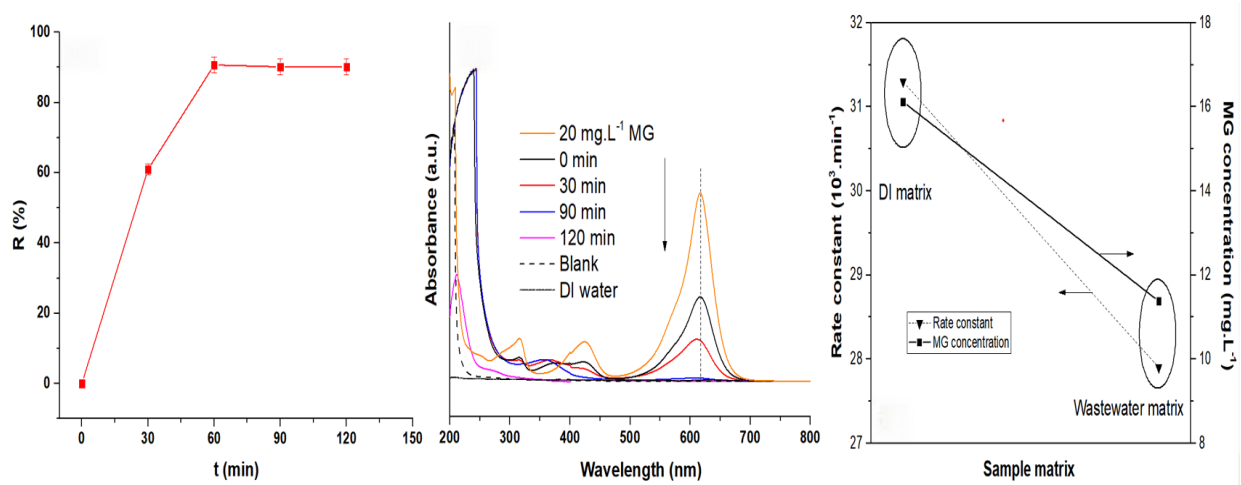

(**a**) (**b**) (**c**)

Figure 8. (**a**) Photodegradation of MG in simulated wastewater (t = 0) using GQD-6@g-C_3N_4 as a catalyst. (**b**) UV-VIS spectra of MG recorded during the photodegradation process; "Blank" corresponds to wastewater without MG addition. (**c**) Influence of sample matrix on the rate constant for MG photodegradation at its respective initial concentrations.

In a fishpond where there is less water exchange, organic compounds, including antibiotics, tend to accumulate in the sediment at the bottom of the pond. The persistent antibiotic residues (e.g., MG) in fishponds may have negative effects on the environment inside the ponds and their surrounding environment. Therefore, the presence of the photocatalysts would boost the abatement of antibiotic residues, which usually take weeks for natural degradation.

4. Conclusion

In this study, we deposited GQDs with varied sizes on the g-C_3N_4 photocatalyst. The process of incorporation of GQDs resulted in the band gaps of the GQDs-loaded g-C_3N_4 samples becoming narrower, which increased the light absorption ability of GQDs-loaded g-C_3N_4 photocatalysts. The results showed that the decoration of g-C_3N_4 with GQDs resulted in the enhancement of MG abatement from the solution, in which O_2^- was the dominant radical. GQD size had a strong influence on the structure and photocatalytic activity of photocatalysts. While their size influences the initial kinetics, the final efficiency tends to converge. GQDs, with an average size of 22 nm, exhibited favorable structural properties and provided optimal photocatalytic performance when incorporated into g-C_3N_4 photocatalysts. In addition to the photocatalysis, the photolysis of MG also took place and was favorable at the alkaline conditions. The study suggested the potential application of *GQDs-loaded* g-C_3N_4 photocatalysts to abate MG in fish-farming-wastewater simulated effluent using UV-driven wastewater treatment systems. However, the impact of ions present in the wastewater matrix on the photocatalytic process and the overall toxicity of the treated wastewater have not yet been examined and should be addressed in future studies.

Supplementary Materials

The supporting information can be downloaded at https://journals.bilpubgroup.com/files/RE-13127-Supplementary-Materials.docx.

Author Contributions

Conceptualization, N.L.M.T.; methodology, D.M.L. and N.L.M.T.; formal analysis, N.L.M.T. and N.T.P.T.;

investigation, D.M.L., N.L.M.T., N.T.P.T., N.V.T., T.T.K. and T.T.H.; resources, N.T.P.T.; data curation, D.M.L., N.L.M.T., N.T.P.T. and N.V.T.; writing—original draft preparation, D.M.L., N.L.M.T., N.T.P.T., N.V.T., T.T.K. and T.T.H.; writing—review and editing, N.L.M.T.; visualization, N.V.T., T.T.K. and T.T.H.; validation, N.T.P.T. All authors have read and agreed to the published version of the manuscript.

Funding

This research is funded by Vietnam National University-Ho Chi Minh City (VNU-HCM) under grant number C2023-24-01.

Institutional Review Board Statement

Not applicable.

Informed Consent Statement

Not applicable.

Data Availability Statement

Any data related to this study will be made available upon reasonable request.

Conflicts of Interest

The authors declare that they have no known competing financial conflicts of interest or personal relationship conflicts of interest that could have appeared to influence the work reported in this paper.

AI Use Statement

The authors declare that no artificial intelligence (AI) tools were used in the preparation of this manuscript.

References

[1] Haji Azaman, S.A., Afandi, A., Hameed, B.H., et al., 2018. Removal of Malachite Green from Aqueous Phase Using Coconut Shell Activated Carbon: Adsorption, Desorption, and Reusability Studies. Journal of Applied Science and Engineering. 21(3), 317–330.

[2] Tkaczyk, A., Mitrowska, K., Posyniak, A., et al., 2020. Synthetic Organic Dyes as Contaminants of the Aquatic Environment and Their Implications for Ecosystems: A Review. Science of the Total Environment. 717, 137222. DOI: https://doi.org/10.1016/j.scitotenv.2020.137222

[3] Sarhadi, T., Rahmani, M., 2024. Assessment of Vortex-Assisted Supramolecular-Based Micro-Extraction for Analysis of Malachite Green in Water Samples. Results in Chemistry. 12, 101905. DOI: https://doi.org/10.1016/j.rechem.2024.101905

[4] Himanshi, Lal, B., Verma, A., et al., 2025. Insights into the Photocatalytic Removal of Malachite Green Organic Pollutant by Highly Efficient Hard Responsive $Ba_{1-x}Co_xDy_\gamma Fe_{12-\gamma}O_{19}$ Catalysts. Scientific Reports. 15(1), 1225. DOI: https://doi.org/10.1038/s41598-024-84251-0

[5] Khodabakhshi, A., Amin, M.M., 2012. Determination of Malachite Green in Trout Tissue and Effluent Water from Fish Farms. International Journal of Environmental Health Engineering. 1(1), 10. DOI: https://doaj.org/article/a1aafe0d27964207b41e1dc2a8087c21

[6] Kwan, P.P., Banerjee, S., Shariff, M., et al., 2018. Quantitative Analysis of Malachite Green and Leucomalachite Green Residues in Fish Purchased From the Markets in Malaysia. Food Control. 92, 101–106. DOI: https://doi.org/10.1016/j.foodcont.2018.04.031

[7] Abed Almonem, K.I., El-Ashgar, N.M., Gahal, A.A., et al., 2022. Applications of Potentiometric Sensors for the Determination of Malachite Green Dye in Real Samples. Sensors International. 3, 100186. DOI: https://doi.org/10.1016/j.sintl.2022.100186

[8] Sadiq, A.C., Olasupo, A., Rahim, N.Y., et al., 2021. Comparative Removal of Malachite Green Dye from Aqueous Solution Using Deep Eutectic Solvents Modified Magnetic Chitosan Nanoparticles and Modified Protonated Chitosan Beads. Journal of Environmental Chemical Engineering. 9(5), 106281. DOI: https://doi.org/10.1016/j.jece.2021.106281

[9] Balasurya, S., Okla, M.K., Mohebaldin, A., et al., 2022. Self-Assembling of 3D Layered Flower Architecture of BiOI Modified $MgCr_2O_4$ Nanosphere for Wider Spectrum Visible-Light Photocatalytic Degradation of Rhodamine B and Malachite Green: Mechanism, Pathway, Reactive Sites and Toxicity Prediction. Journal of Environmental Management. 308, 114614. DOI: https://doi.org/10.1016/j.jen-

vman.2022.114614

[10] Kien, T.T., Linh, D.M., Hung, N.T., et al., 2023. Nitrogen Source Recovery Efficiency in the Catfish Farming Zero-Emission Integrated System in the Mekong Delta, Viet Nam. Journal of Environmental Chemical Engineering. 11(2), 109452. DOI: https://doi.org/10.1016/j.jece.2023.109452

[11] Henares, M.N.P., Medeiros, M.V., Camargo, A.F.M., et al., 2020. Overview of Strategies That Contribute to the Environmental Sustainability of Pond Aquaculture: Rearing Systems, Residue Treatment, and Environmental Assessment Tools. Reviews in Aquaculture. 12(1), 453–470. DOI: https://doi.org/10.1111/raq.12327

[12] Khan, N.A., Khan, A.H., Tiwari, P., et al., 2021. New Insights into the Integrated Application of Fenton-Based Oxidation Processes for the Treatment of Pharmaceutical Wastewater. Journal of Water Process Engineering. 44, 102440. DOI: https://doi.org/10.1016/j.jwpe.2021.102440

[13] Gabris, M.A., Periyasamy, A.P., Tehrani-Bagha, A., et al., 2025. Top Ten Super-Adsorbents for Removal of Textile Dyes from Wastewater. Environmental Research. 285, 122424. DOI: https://doi.org/10.1016/j.envres.2025.122424

[14] Banyal, R., Khan, A.A.P., Sudhaik, A., et al., 2023. Emergence of $CuInS_2$-Derived Photocatalysts for Environmental Remediation and Energy Conversion. Environmental Research. 238, 117288. DOI: https://doi.org/10.1016/j.envres.2023.117288

[15] Albukhari, S.M., Ismail, A.A., 2024. Synthesis of Mesoporous p-$CuAl_2O_4$/n-YVO_4 Heterojunction Nanocomposites and Their Utilization as Effective Photocatalysts for Hydrogen Evolution. Fuel. 357, 129755. DOI: https://doi.org/10.1016/j.fuel.2023.129755

[16] Kadkhodayan, H., Alizadeh, T., 2023. Manufacturing Visible-Light-Driven Heterojunction Photocatalyst Based on MOFs/$Bi_2WZnTiO_9$ Triple Perovskite/Carbonous Materials for Efficient Removal of Poisons, Antibiotics, and Inorganic Pollutants. Journal of Physics and Chemistry of Solids. 183, 111620. DOI: https://doi.org/10.1016/j.jpcs.2023.111620

[17] Mohammed, R.O., Amooey, A.A., Ammar, S.H., et al., 2023. Enhanced Photocatalytic Degradation Activity of ZIF-8 Doped with Ag_2WO_4 Photocatalyst. Journal of the Taiwan Institute of Chemical Engineers. 151, 105141. DOI: https://doi.org/10.1016/j.jtice.2023.105141

[18] Singh, R., Chauhan, M., Garg, P., et al., 2023. A Critical Review on Visible Light Active Graphitic Carbon Nitride (g-CN) Based Photocatalyst for Environment Remediation Application: A Sustainable Approach. Journal of Cleaner Production. 427, 138855. DOI: https://doi.org/10.1016/j.jclepro.2023.138855

[19] Vinoth, S., Shalini Devi, K.S., Pandikumar, A., et al., 2021. A Comprehensive Review on Graphitic Carbon Nitride Based Electrochemical and Biosensors for Environmental and Healthcare Applications. TrAC Trends in Analytical Chemistry. 140, 116274. DOI: https://doi.org/10.1016/j.trac.2021.116274

[20] Wen, J., Xie, J., Chen, X., et al., 2017. A Review on g-C_3N_4-Based Photocatalysts. Applied Surface Science. 391, 72–123. DOI: https://doi.org/10.1016/j.apsusc.2016.07.030

[21] Bang Truong, H., Cuong Nguyen, X., Hur, J., et al., 2023. Recent Advances in g-C_3N_4-Based Photocatalysis for Water Treatment: Magnetic and Floating Photocatalysts, and Applications of Machine-Learning Techniques. Journal of Environmental Management. 345, 118895. DOI: https://doi.org/10.1016/j.jenvman.2023.118895

[22] Lin, X., Liu, C., Wang, J., et al., 2019. Graphitic Carbon Nitride Quantum Dots and Nitrogen-Doped Carbon Quantum Dots Co-Decorated with $BiVO_4$ Microspheres: A Ternary Heterostructure Photocatalyst for Water Purification. Separation and Purification Technology. 226, 117–127. DOI: https://doi.org/10.1016/j.seppur.2019.05.093

[23] Wang, Y., Yang, Z., Zhang, C., et al., 2023. Fabricating Carbon Quantum Dots of Graphitic Carbon Nitride Vis Ultrasonic Exfoliation for Highly Efficient H_2O_2 Production. Ultrasonics Sonochemistry. 99, 106582. DOI: https://doi.org/10.1016/j.ultsonch.2023.106582

[24] Balakumar, V., Ramalingam, M., Sekar, K., et al., 2021. Fabrication and Characterization of Carbon Quantum Dots Decorated Hollow Porous Graphitic Carbon Nitride through Polyaniline for Photocatalysis. Chemical Engineering Journal. 426, 131739. DOI: https://doi.org/10.1016/j.cej.2021.131739

[25] Molaei, M.J., 2023. Graphitic Carbon Nitride (g-C_3N_4) Synthesis and Heterostructures, Principles, Mechanisms, and Recent Advances: A Critical Review. International Journal of Hydrogen Energy. 48(84), 32708–32728. DOI: https://doi.org/10.1016/j.ijhydene.2023.05.066

[26] Kharangarh, P.R., Ravindra, N.M., Singh, G., et al., 2023. Synthesis of Luminescent Graphene Quantum Dots from Biomass Waste Materials for Energy-Related Applications: An Overview. Energy Storage. 5(3), e390. DOI: https://doi.org/10.1002/est2.390

[27] Lopez-Picazo, P.I., Sanchez-Tizapa, M., Tostado-Plascencia, M.M., et al., 2023. Characterization of Sensitized Solar Cells Based on Nanocomposites of Protoporphyrin IX and Microwave Reduced Graphene Oxide Quantum Dots. Diamond and Related Materials. 139, 110337. DOI: https://doi.org/10.1016/j.diamond.2023.110337

[28] Ajeel, F.N., Mohsin, K.H., Shakier, H.G., et al., 2023. Theoretical Insights into Tunable Electronic Properties of Graphene Quantum Dots through ZnO Doping. Chemical Physics Impact. 7, 100305. DOI: https://doi.org/10.1016/j.chphi.2023.100305

[29] Turunc, E., Kahraman, O., Dogen, A., et al., 2023. Green Synthesis of Graphene Quantum Dot- and Its Electrochemical, Antioxidant and Antimicrobial Activities. Synthetic Metals. 299, 117453. DOI: https://doi.org/10.1016/j.synthmet.2023.117453

[30] Roy, E., Nagar, A., Sharma, A., et al., 2021. Graphene Quantum Dots and Its Modified Application for Energy Storage and Conversion. Journal of Energy Storage. 39, 102606. DOI: https://doi.org/10.1016/j.est.2021.102606

[31] Tian, P., Tang, L., Teng, K.S., et al., 2018. Graphene Quantum Dots from Chemistry to Applications. Materials Today Chemistry. 10, 221–258. DOI: https://doi.org/10.1016/j.mtchem.2018.09.007

[32] Ma, W., Wang, J., Wu, T., et al., 2023. Three-Dimensional Nitrogen-Doped Graphene Quantum Dots/Reduced Graphene Oxide Composite Hydrogels as Binder-Free Electrodes for Symmetric Supercapacitors. Materials Chemistry and Physics. 310, 128365. DOI: https://doi.org/10.1016/j.matchemphys.2023.128365

[33] Phuong Thao, N.T., Le Minh Tri, N., Kien, T.T., et al., 2024. Valorization of Antibiotic and Organic Wastewater Using Graphene Quantum Dots Deposited g-C_3N_4 Photocatalysts. Heliyon. 10(5), e26783. DOI: https://doi.org/10.1016/j.heliyon.2024.e26783

[34] Huang, W., Li, X., Sun, X., et al., 2021. Photoluminescence Enhancement of Graphene Quantum Dots by Microwave Post-Treatment. Chemical Engineering Journal. 405, 126714. DOI: https://doi.org/10.1016/j.cej.2020.126714

[35] Masoumi Sangani, M.M., Shahin, M.S., Yavari, M.A., et al., 2024. Tailoring Photocatalytic Activity of g-C_3N_4 Using Sulfanilic Acid and Chitosan Beads for Cr(VI) Removal. Journal of Industrial and Engineering Chemistry. 130, 412–424. DOI: https://doi.org/10.1016/j.jiec.2023.09.047

[36] Abebe, H.A., Diro, A., Kitte, S.A., et al., 2023. Voltammetric Determination of Tryptophan at Graphitic Carbon Nitride Modified Carbon Paste Electrode. Heliyon. 9(10), e21033. DOI: https://doi.org/10.1016/j.heliyon.2023.e21033

[37] Bankole, O.M., Olorunsola, T.D., Ogunlaja, A.S., et al., 2021. Photocatalytic Decontamination of Hexavalent Chromium over g-C_3N_4 Supported Sulfur Nanoparticles. Journal of Photochemistry and Photobiology A: Chemistry. 405, 112934. DOI: https://doi.org/10.1016/j.jphotochem.2020.112934

[38] Hao, M., Li, Y., Gao, L., et al., 2020. In-Situ Hard Template Synthesis of Mesoporous Carbon/Graphite Carbon Nitride (C/CN-T-x) Composites With High Photocatalytic Activities under Visible Light Irridation. Solid State Sciences. 109, 106428. DOI: https://doi.org/10.1016/j.solidstatesciences.2020.106428

[39] Jiao, Y., Huang, Q., Wang, J., et al., 2019. A Novel MoS_2 Quantum Dots (QDs) Decorated Z-Scheme g-C_3N_4 Nanosheet/N-Doped Carbon Dots Heterostructure Photocatalyst for Photocatalytic Hydrogen Evolution. Applied Catalysis B: Environmental. 247, 124–132. DOI: https://doi.org/10.1016/j.apcatb.2019.01.073

[40] Llaver, M., Barrionuevo, S.D., Prieto, E., et al., 2022. Functionalized Graphene Quantum Dots Obtained From Graphene Foams Used for Highly Selective Detection of Hg^{2+} in Real Samples. Analytica Chimica Acta. 1232, 340422. DOI: https://doi.org/10.1016/j.aca.2022.340422

[41] Mohammed-Ahmed, H.K., Nakipoglu, M., Tezcaner, A., et al., 2023. Functionalization of Graphene Oxide Quantum Dots for Anticancer Drug Delivery. Journal of Drug Delivery Science and Technology. 80, 104199. DOI: https://doi.org/10.1016/j.jddst.2023.104199

[42] Chen, H., Liu, T., Meng, Y., et al., 2020. Novel Graphene Oxide/Aminated Lignin Aerogels for Enhanced Adsorption of Malachite Green in Wastewater. Colloids and Surfaces A: Physicochemical and Engineering Aspects. 603, 125281. DOI: https://doi.org/10.1016/j.colsurfa.2020.125281

[43] Oladoye, P.O., Ajiboye, T.O., Wanyonyi, W.C., et al., 2023. Insights into Remediation Technology for Malachite Green Wastewater Treatment. Water Science and Engineering. 16(3), 261–270. DOI: https://doi.org/10.1016/j.wse.2023.03.002

[44] Bui, T.S., Bansal, P., Lee, B.-K., et al., 2020. Facile Fabrication of Novel Ba-Doped g-C_3N_4 Photocatalyst with Remarkably Enhanced Photocatalytic Activity towards Tetracycline Elimination under Visible-Light Irradiation. Applied Surface Science. 506, 144184. DOI: https://doi.org/10.1016/j.apsusc.2019.144184

[45] Chen, C.C., Lu, C.S., Chung, Y.C., et al., 2007.

UV-Induced Photodegradation of Malachite Green on TiO_2 Nanoparticles. Journal of Hazardous Materials. 141(3), 520–528. DOI: https://doi.org/10.1016/j.jhazmat.2006.07.011

[46] Madona, J., Sridevi, C., Indumathi, N., et al., 2024. A Novel Carbon Doped CeO_2/g-C_3N_4 Heterostructure for Disinfection of Microorganisms and Degradation of Malachite Green and Amoxicillin under Sunlight. Surfaces and Interfaces. 44, 103803. DOI: https://doi.org/10.1016/j.surfin.2023.103803

[47] Shaheen, N., Warsi, M.F., Zulfiqar, S., et al., 2023. Carbon Coated Tungsten Doped Molybdenum Oxide Nanowires and Their Composite with Graphitic Carbon Nitride for Photocatalysis and Antibacterial Studies. Ceramics International. 49(4), 6906–6922. DOI: https://doi.org/10.1016/j.ceramint.2022.10.076

[48] Hasija, V., Raizada, P., Sudhaik, A., et al., 2020. Fabrication of Ag/AgI/WO_3 Heterojunction Anchored P and S Co-Doped Graphitic Carbon Nitride as a Dual Z Scheme Photocatalyst for Efficient Dye Degradation. Solid State Sciences. 100, 106095. DOI: https://doi.org/10.1016/j.solidstatesciences.2019.106095

[49] Mohanty, L., Sundar Pattanayak, D., Singhal, R., et al., 2022. Enhanced Photocatalytic Degradation of Rhodamine B and Malachite Green Employing $BiFeO_3$/g-C_3N_4 Nanocomposites: An Efficient Visible-Light Photocatalyst. Inorganic Chemistry Communications. 138, 109286. DOI: https://doi.org/10.1016/j.inoche.2022.109286

[50] Salehzadeh, J., Nassiri, M., Dehghani, Z., et al., 2025. Synthesis of TiO_2 Nanoparticles: Structural Characterization, Photocatalytic Degradation of Malachite Green Dye from Aqueous Solution under UV Irradiation. Journal of the Indian Chemical Society. 102(10), 102059. DOI: https://doi.org/10.1016/j.jics.2025.102059

[51] Rout, D.R., Chaurasia, S., Jena, H.M., et al., 2022. Enhanced Photocatalytic Degradation of Malachite Green Using Manganese Oxide Doped Graphene Oxide/Zinc Oxide (GO-ZnO/Mn_2O_3) Ternary Composite under Sunlight Irradiation. Journal of Environmental Management. 318, 115449. DOI: https://doi.org/10.1016/j.jenvman.2022.115449

[52] Zhang, J., Zhao, Y., Qi, K., et al., 2024. $CuInS_2$ Quantum-Dot-Modified g-C_3N_4 S-Scheme Heterojunction Photocatalyst for Hydrogen Production and Tetracycline Degradation. Journal of Materials Science & Technology. 172, 145–155. DOI: https://doi.org/10.1016/j.jmst.2023.06.042

[53] Bhanderi, D., Lakhani, P., Modi, C.K., et al., 2024. Graphitic Carbon Nitride (g-C_3N_4) as an Emerging Photocatalyst for Sustainable Environmental Applications: A Comprehensive Review. RSC Sustainability. 2(2), 265–287. DOI: https://doi.org/10.1039/d3su00382e

[54] Zhou, Y., Zhang, L., Huang, W., et al., 2016. N-Doped Graphitic Carbon-Incorporated g-C_3N_4 for Remarkably Enhanced Photocatalytic H_2 Evolution under Visible Light. Carbon. 99, 111–117. DOI: https://doi.org/10.1016/j.carbon.2015.12.008

[55] Yong, L., Zhanqi, G., Yuefei, J., et al., 2015. Photodegradation of Malachite Green under Simulated and Natural Irradiation: Kinetics, Products, and Pathways. Journal of Hazardous Materials. 285, 127–136. DOI: https://doi.org/10.1016/j.jhazmat.2014.11.041

[56] Lv, G., Zhang, Z., Shen, Y., et al., 2024. Biodegradation of Malachite Green by *Pleurotus eryngii*: A Study on Decolorization, Mechanism, Toxicity, and Enzyme. Environmental Science and Pollution Research. 31(13), 20084–20092. DOI: https://doi.org/10.1007/s11356-024-32465-0

[57] Lin, F., Song, S., Liu, L., et al., 2011. Detection of Benzophenone in Recycled Paper Packaging by ELISA. Food and Agricultural Immunology. 22(1), 39–46. DOI: https://doi.org/10.1080/09540105.2010.523781

[58] Pattanaik, R., Pradhan, D., Kamal, R., et al., 2025. Facile Synthesis of Sr-$Bi_4Ti_3O_{12}$: A Promising Photocatalyst for Enhanced Degradation of Malachite Green Dye under Solar Irradiation. Next Materials. 8, 100847. DOI: https://doi.org/10.1016/j.nxmate.2025.100847

[59] Li, Z., Deng, Y., Zheng, M., et al., 2026. A review of global aquaculture wastewater treatment and management: Sustainable pathways through technological innovations and policy coordination. Journal of Hazardous Materials. 503, 141235. DOI: https://doi.org/10.1016/j.jhazmat.2026.141235